PERGAMON

International Journal of Solids and Structures 39 (2002) 4073–4091

INTERNATIONAL JOURNAL OF SOLIDS and STRUCTURES

www.elsevier.com/locate/ijsolstr

Poroelastic spectral element for wave propagation and parameter identification in multi-layer systems

R. Al-Khoury, C. Kasbergen, A. Scarpas *, J. Blaauwendraad

Faculty of Civil Engineering and Geosciences, Section of Structural Mechanics, Delft University of Technology, Stevinweg 1, 2628 CN Delft, The Netherlands

Received 17 May 2001; received in revised form 6 March 2002

Abstract

This contribution deals with the use of Biot's theory of propagation of elastic waves in a fluid-saturated porous solid in conjunction with the computationally efficient spectral element technique as a means for forward analysis of the dynamic behavior of multi-layer systems consisting of both one- and two-phase material layers. Details of the mathematical formulation and verification of an axi-symmetric semi-infinite spectral element for a fully saturated porous medium are presented. The spatial domain of the element in the vertical direction is assumed to extend to infinity. In the radial direction it extends to a finite distance. In the last part of this contribution an example is presented of the use of the developed element for parameter identification of pavement layers via the use of falling weight deflectometer test. © 2002 Published by Elsevier Science Ltd.

Keywords: Biot's theory; Porous media; Spectral element; Parameter identification technique; Falling weight deflectometer

1. Introduction

In earlier publications (Al-Khoury et al., 2001a,b, part I and II) axi-symmetric spectral elements for layered system have been developed for forward and inverse calculations in one-phase solid media. In the present publication the previous work has been extended to include two-phase porous media. The objective of this research work is the development of a robust and computationally efficient parameter identification technique for layered systems via the use of non-destructive testing. Particular attention is given to the identification of pavement layer parameters via the use of the falling weight deflectometer test (FWD).

Biot's theory of propagation of elastic waves in a fluid-saturated porous solid (Biot, 1956) has been used by a number of researchers as a basis for the development of various solution methods spanning from analytical to finite elements. Analytical methods have been utilized by, among others, Halpern and Christiano (1986), Philippacopoulos (1988), and Zeng and Rajapakse (1999) to study wave propagation under well-defined geometric and loading configurations. Either half space or two-layer systems with either

* Corresponding author. Tel.: +31-15-278-4017; fax: +31-15-278-5767.
E-mail address: a.scarpas@ct.tudelft.nl (A. Scarpas).

0020-7683/02/$ - see front matter © 2002 Published by Elsevier Science Ltd.
PII: S0020-7683(02)00260-3

surface or embedded loads have been studied. The focus of the majority of such work is on the effects of different parameters on the overall response of the porous medium.

Most of the analytical solutions are based on far field formulations, in which it is assumed that the structure has infinite boundaries in the radial direction (in case of cylindrical coordinates r, θ, z). Solution of the governing equations for such problems usually involves Hankel integral transform in the spatial domain as

$$\begin{aligned} \mathbf{u}^{\mathrm{H}}(\xi,z) &= \int_0^\infty r\mathbf{u}(r,z)J_v(\xi r)\,\mathrm{d}r \\ \mathbf{u}(r,z) &= \int_0^\infty \xi\mathbf{u}^{\mathrm{H}}(\xi,z)J_v(\xi r)\,\mathrm{d}\xi \end{aligned} \tag{1}$$

in which $\mathbf{u}(r,z)$ is a displacement function with $\mathbf{u}^{\mathrm{H}}(\xi,z)$ is its Hankel transform, ξ is the wavenumber and J_v is the Bessel function of the first kind of order v. Typically $\mathbf{u}^{\mathrm{H}}(\xi,z)$ forms transcendental functions, which in many situations, cause numerical inconveniences when integrated between zero and infinity (Seale and Kausel, 1989).

Finite element techniques have been intensively utilized by among others, Yan et al. (1999), Khalili et al. (1999) and Liu et al. (2000). Finite element method is a powerful tool suitable for forward calculations of general cases with complicated geometrical and load configurations. However, because of the computational requirements its utilization for inverse calculations is limited.

Semi-analytical methods, on the other hand, represent a combination of analytical and finite element methods. Both exact and semi-discrete stiffness matrices are involved in such techniques. Among others, Senjuntichai and Rajapakse (1995) and Degrande et al. (1998) have formulated exact stiffness matrices for layered poroelastic systems. These formulations require evaluation, numerical or otherwise, of the integrals of Eq. (1).

The semi-discrete stiffness matrix technique, developed by Lysmer (1970) and later generalized by Kausel and Roesset (1981), was utilized by Bougacha et al. (1993) for the analysis of foundations on a poroelastic stratum. The advantage of this technique is the substitution of the transcendental functions, Eq. (1), with algebraic expressions by discretizing the layers involved into many sub-layers by means of linear shape functions in resemblance to that of the finite element technique. This makes the semi-discrete technique more efficient and robust. Whereas this technique is suitable for forward calculations, its computational requirements, however, can be quite significant mainly when utilized in iterative schemes for inverse calculations.

Another class of the semi-analytical methods is the spectral element technique introduced by Doyle (1997). The spectral layer elements are described by exact stiffness matrices similar to those mentioned above. However, unlike these, which impose continuity of displacements at the layer boundaries (e.g. $u(r,z_j^-) = u(r,z_j^+)$), the conditions at the boundaries between layers are defined by element nodes similar to that in the finite element method. At the element node, the degrees of freedom are specified and numbered locally regardless of the neighboring layers. The assembly of the layers is done according to the conventional finite element techniques. This renders the spectral element method more general and suitable for a wider range of engineering problems (Rizzi and Doyle, 1992). The generality implies that the load can be applied at the surface and/or at any other layer boundary, the bottom boundary can be rigid or infinite, etc. Degrande and De Roeck (1992) have utilized the spectral element method for the formulation of plain strain spectral elements for porous media.

In this contribution, and because of the computational advantages of the spectral element method, an axi-symmetric semi-infinite spectral element for porous media is derived. To improve further the computational efficiency, the following boundary conditions are imposed:

1. The element is assumed to extend to infinity in the vertical direction, z, and to a finite distance, where waves are known a priori to vanish, in the radial direction, r. The later condition leads to a series summation, alleviating thus, the inconvenience of the infinite integration (Eq. (1)).
2. Drained conditions are assumed at the top surface of the element. The imposition of this condition allows formulation of the stiffness matrix of the element in terms of the two degrees of freedom of the solid component (like that of the one-phase) reducing thus the overall size of the system matrix manipulations.

Also, in this contribution, a parameter identification procedure proposed earlier (Al-Khoury et al., 2001a,b) has been adopted to the case of layer systems consisting of both dry and saturated layers. This procedure, in combination with the forward model, enables parameter identification of layered systems on the basis of experimentally measured data. In the last part of the contribution an example is presented for parameter identification of pavement layers via the use of FWD test.

2. The governing equations

The equations of motion for a homogeneous isotropic poroelastic solid governed by Biot's two-phase theory may be expressed as:

$$\begin{aligned} \sigma_{ij,j} &= \rho_{11}\ddot{u}_{si}, + \rho_{12}\ddot{u}_{fi} + b(\dot{u}_{si} - \dot{u}_{fi}) \\ \sigma_{,i} &= \rho_{12}\ddot{u}_{si} + \rho_{22}\ddot{u}_{fi} - b(\dot{u}_{si} - \dot{u}_{fi}) \end{aligned} \tag{2}$$

in which $\sigma = -\phi p$ (where p is the fluid pressure and ϕ is the porosity) represents the stress which acts on the fluid phase, while σ_{ij} is the tensor of the stresses which act on the solid phase of the material. u_{si} and u_{fi} are the displacement vectors of the solid and fluid phases respectively. $b = (\gamma/\kappa)\phi^2$ (where γ is the fluid unit weight and κ is the permeability) represents the dissipation factor which controls the relative motion between fluid and solid. The density coefficients $\rho_{11} = \rho + \phi\rho_f(a-2)$, $\rho_{12} = \phi\rho_f(1-a)$, $\rho_{22} = \tilde{a}\phi\rho_f$ (where $\tilde{a}$ is Biot's tortuosity parameter, Bourbie et al., 1987), represent the total effective mass of solid moving in the fluid and their coupling (Biot, 1956). (The tilde ($\tilde{\cdot}$) will be used in this paper to indicate Biot's parameters.) $\rho = (1-\phi)\rho_s + \phi\rho_f$ is the conventional density of porous media where ρ_s and ρ_f are the solid (skeleton) and fluid densities respectively.

For an axi-symmetric porous solid, the stress–strain relations are (Biot, 1956)

$$\begin{aligned} \sigma_{rr} &= 2\mu e_{rr} + \tilde{\lambda}e + \tilde{Q}\varepsilon \\ \sigma_{zz} &= 2\mu e_{zz} + \tilde{\lambda}e + \tilde{Q}\varepsilon \\ \sigma_{\theta\theta} &= 2\mu e_{\theta\theta} + \tilde{\lambda}e + \tilde{Q}\varepsilon \\ \tau_{rz} &= \mu e_{rz} \\ \sigma &= \tilde{Q}e + \tilde{R}\varepsilon \end{aligned} \tag{3}$$

in which $e_{rr} = (\partial u_s/\partial r)$, $e_{zz} = (\partial w_s/\partial z)$, $e_{rz} = (\partial u_s/\partial z) + (\partial w_s/\partial r)$ and $e_{\theta\theta} = (u_s/r)$ (where u_s and w_s are the radial and vertical displacements of the solid phase respectively) represent the strain components in the solid phase and $e = e_{rr} + e_{zz} + e_{\theta\theta}$ represents the dilation of the solid. $\varepsilon = (\partial u_f/\partial r) + (\partial w_f/\partial z) + (u_f/r)$ (where u_f and w_f are the radial and vertical displacements of the fluid phase respectively) represents the dilation of the fluid. The material parameters of Eq. (3) are defined as (Bourbie et al., 1987): μ the shear modulus of the material, $\tilde{\lambda} = \lambda + (\tilde{Q}^2/\tilde{R})$, $\tilde{Q} = \tilde{M}\phi(\tilde{\beta} - \phi)$ and $\tilde{R} = \tilde{M}\phi^2$ in which λ is the Lame' coefficient for the drained case, $\tilde{M}$ is the Biot's coefficient for the compressibility of the two-phase material and $\tilde{\beta}$ is Biot's coefficient for the fluid flow which is a function of porosity and the geometry of the channels where

flow occurs. Details of the parameter identification and experimental determination can be found in Biot and Willis (1957).

Upon substituting Eq. (3) into Eq. (2), the governing equations of motion in terms of displacements can be obtained as

$$\begin{aligned}&(\tilde{\lambda}+2\mu)\nabla\nabla\cdot\mathbf{u}_{\mathrm{s}}+\tilde{Q}\nabla\nabla\cdot\mathbf{u}_{\mathrm{f}}+,\mu\nabla\times\nabla\times\mathbf{u}_{\mathrm{s}}=\rho_{11}\ddot{\mathbf{u}}_{\mathrm{s}}+\rho_{12}\ddot{\mathbf{u}}_{\mathrm{f}}+b(\dot{\mathbf{u}}_{\mathrm{s}}-\dot{\mathbf{u}}_{\mathrm{f}})\\&\tilde{Q}\nabla\nabla\cdot\mathbf{u}_{\mathrm{s}}+\tilde{R}\nabla\nabla\cdot\mathbf{u}_{\mathrm{f}}=\rho_{12}\ddot{\mathbf{u}}_{\mathrm{s}}+\rho_{22}\ddot{\mathbf{u}}_{\mathrm{f}}-b(\dot{\mathbf{u}}_{\mathrm{s}}-\dot{\mathbf{u}}_{\mathrm{f}})\end{aligned}\tag{4}$$

For an axi-symmetric case, Eq. (4) represents four coupled equations for the four unknown displacements $\mathbf{u}_{\mathrm{s}}$ and $\mathbf{u}_{\mathrm{f}}$. As in the case of one-phase solid, by means of Helmholtz decomposition, the displacement fields corresponding to the solid and the liquid components can be expressed as the sum of the gradient of a scalar potential φ and the curl of a vector potential $\boldsymbol{\psi}$ as (Biot, 1956; Halpern and Christiano, 1986)

$$\begin{aligned}\mathbf{u}_{\mathrm{s}}&=\nabla\varphi_{\mathrm{s}}+\nabla\times\boldsymbol{\psi}_{\mathrm{s}}\\\mathbf{u}_{\mathrm{f}}&=\nabla\varphi_{\mathrm{f}}+\nabla\times\boldsymbol{\psi}_{\mathrm{f}}\end{aligned}\tag{5}$$

In an axi-symmetric motion, the vector potential $\boldsymbol{\psi}$ has a component ψ_θ only. Thus $\nabla^2\boldsymbol{\psi}=\nabla^2\psi_\theta-(\psi_\theta/r^2)$. This property reduces the solution of the problem to solving only for scalar potentials. For convenience of notation, ψ will be written instead of ψ_θ.

By substituting Eq. (5) into Eq. (4) and applying the condition $\nabla\cdot\boldsymbol{\psi}=0$ (Achenbach, 1973), the following equations of motion are obtained:

$$\begin{aligned}&\nabla\left[\left(\tilde{\lambda}+2\mu\right)\nabla^2\varphi_{\mathrm{s}}+\tilde{Q}\nabla^2\varphi_{\mathrm{f}}-\rho_{11}\ddot{\varphi}_{\mathrm{s}}-\rho_{12}\ddot{\varphi}_{\mathrm{f}}-b\dot{\varphi}_{\mathrm{s}}+b\dot{\varphi}_{\mathrm{f}}\right]\\&\quad+\nabla\left[\mu\left(\nabla^2\psi_{\mathrm{s}}-\frac{\psi_{\mathrm{s}}}{r^2}\right)-\rho_{11}\ddot{\psi}_{\mathrm{s}}-\rho_{12}\ddot{\psi}_{\mathrm{f}}-b\dot{\psi}_{\mathrm{s}}+b\dot{\psi}_{\mathrm{f}}\right]=0\\&\nabla\left[\tilde{Q}\nabla^2\varphi_{\mathrm{s}}+\tilde{R}\nabla^2\varphi_{\mathrm{f}}-\rho_{12}\ddot{\varphi}_{\mathrm{s}}-\rho_{22}\ddot{\varphi}_{\mathrm{f}}+b\dot{\varphi}_{\mathrm{s}}-b\dot{\varphi}_{\mathrm{f}}\right]+\nabla\left[-\rho_{12}\ddot{\psi}_{\mathrm{s}}-\rho_{22}\ddot{\psi}_{\mathrm{f}}+b\dot{\psi}_{\mathrm{s}}-b\dot{\psi}_{\mathrm{f}}\right]=0\end{aligned}\tag{6}$$

These equations will be satisfied if each bracketed term vanishes, hence, Eq. (6) yields two uncoupled sets of simultaneous equations as

$$\left.\begin{aligned}(\tilde{\lambda}+2\mu)\nabla^2\varphi_{\mathrm{s}}+\tilde{Q}\nabla^2\varphi_{\mathrm{f}}-\rho_{11}\ddot{\varphi}_{\mathrm{s}}-\rho_{12}\ddot{\varphi}_{\mathrm{f}}-b(\dot{\varphi}_{\mathrm{s}}-\dot{\varphi}_{\mathrm{f}})=0\\\tilde{Q}\nabla^2\varphi_{\mathrm{s}}+\tilde{R}\nabla^2\varphi_{\mathrm{f}}-\rho_{12}\ddot{\varphi}_{\mathrm{s}}-\rho_{22}\ddot{\varphi}_{\mathrm{f}}+b(\dot{\varphi}_{\mathrm{s}}-\dot{\varphi}_{\mathrm{f}})=0\end{aligned}\right\}\tag{7a}$$

$$\left.\begin{aligned}\mu\left(\nabla^2\psi_{\mathrm{s}}-\tfrac{\psi_{\mathrm{s}}}{r^2}\right)-\rho_{11}\ddot{\psi}_{\mathrm{s}}-\rho_{12}\ddot{\psi}_{\mathrm{f}}-b(\dot{\psi}_{\mathrm{s}}-\dot{\psi}_{\mathrm{f}})=0\\-\rho_{12}\ddot{\psi}_{\mathrm{s}}-\rho_{22}\ddot{\psi}_{\mathrm{f}}+b(\dot{\psi}_{\mathrm{s}}-\dot{\psi}_{\mathrm{f}})=0\end{aligned}\right\}\tag{7b}$$

In analogy to the case of the one-phase continuum medium, Eqs. (7a) and (7b) describe attenuated dilatational and rotational waves in a porous medium respectively.

Applying Fourier transform to Eqs. (7a) and (7b) yields

$$\left.\begin{aligned}(\tilde{\lambda}+2\mu)\nabla^2\hat{\varphi}_{\mathrm{s}}+\tilde{Q}\nabla^2\hat{\varphi}_{\mathrm{f}}=M_{11}\hat{\varphi}_{\mathrm{s}}+M_{12}\hat{\varphi}_{\mathrm{f}}\\\tilde{Q}\nabla^2\hat{\varphi}_{\mathrm{s}}+\tilde{R}\nabla^2\hat{\varphi}_{\mathrm{f}}=M_{12}\hat{\varphi}_{\mathrm{s}}+M_{22}\hat{\varphi}_{\mathrm{f}}\end{aligned}\right\}\tag{8a}$$

$$\left.\begin{aligned}\mu\left(\nabla^2\hat{\psi}_{\mathrm{s}}-\tfrac{\hat{\psi}_{\mathrm{s}}}{r^2}\right)=M_{11}\hat{\psi}_{\mathrm{s}}+M_{12}\hat{\psi}_{\mathrm{f}}\\0=M_{12}\hat{\psi}_{\mathrm{s}}+M_{22}\hat{\psi}_{\mathrm{f}}\end{aligned}\right\}\tag{8b}$$

in which $M_{11} = -\omega^2\rho_{11} + \mathrm{i}\omega b$, $M_{12} = -\omega^2\rho_{12} - \mathrm{i}\omega b$ and $M_{22} = -\omega^2\rho_{22} + \mathrm{i}\omega b$ where ω is the angular frequency and $\mathrm{i} = \sqrt{-1}$. The hat $(\hat{\cdot})$ in Eqs. (8a) and (8b) indicate the frequency domain formulation. Eq. (8a) reveals the existence of two dilatational waves and that each of these waves involves coupled motion in the fluid and the solid. While Eq. (8b) reveals the existence of one rotational wave due to the solid phase with a coupling of motion between the solid and fluid (Biot, 1956).

2.1. Solution of the rotational waves

From the second expression of Eq. (8b) it can be seen that

$$\hat{\psi}_\mathrm{f} = -\frac{M_{12}}{M_{22}}\hat{\psi}_\mathrm{s} \tag{9}$$

Substituting Eq. (9) into the first expression of Eq. (8b) yields

$$\mu\left(\nabla^2\hat{\psi}_\mathrm{s} - \frac{\hat{\psi}_\mathrm{s}}{r^2}\right) = M_0\hat{\psi}_\mathrm{s} \tag{10}$$

in which $M_0 = M_{11} - (M_{12}^2/M_{22})$. Eq. (10), can be solved by the method of separation of variables, resulting to

$$\hat{\psi}_\mathrm{s}(\omega,\xi,r,z) = H_z J_1(\xi r) \tag{11}$$

where ξ is the wavenumber in the radial direction and J_1 is the Bessel function of the first kind of order one. By substituting Eq. (11) into Eq. (10), the solution of the resulting ordinary differential equation is

$$H_z = A\mathrm{e}^{-\zeta_\mathrm{sh}z} \tag{12}$$

in which $\zeta_\mathrm{sh} = ((M_0/\mu) + \xi^2)^{1/2}$ and the subscript sh refers to the shear (rotational) wave. (The second solution of Eq. (12) ($B\mathrm{e}^{\zeta_\mathrm{sh}z}$) has been discarded to keep the solution finite in large depths.) Therefore, the solution of the rotational wave is

$$\begin{aligned}\hat{\psi}_\mathrm{s}(\omega,\xi,r,z) &= A\mathrm{e}^{-\zeta_\mathrm{sh}z}J_1(\xi r)\\ \hat{\psi}_\mathrm{f}(\omega,\xi,r,z) &= -A\frac{M_{12}}{M_{22}}\mathrm{e}^{-\zeta_\mathrm{sh}z}J_1(\xi r)\end{aligned} \tag{13}$$

By letting $\rho_{12} = \rho_{22} = 0$ and $\rho_{11} = \rho$, the exponent $\zeta_\mathrm{sh} = ((M_0/\mu) + \xi^2)^{1/2}$ in Eq. (13) reduces to $\zeta_\mathrm{sh} = (-(\omega^2/c_\mathrm{sh}^2) + \xi^2)^{1/2}$ in which $c_\mathrm{sh}^2 = \mu/\rho$ as that for the rotational waves in one-phase media (Al-Khoury et al., 2001a,b).

2.2. Solution of the dilatational waves

The two expressions in Eq. (8a) can be presented in a matrix format as

$$\begin{bmatrix}\tilde{\lambda}+2\mu & \tilde{Q}\\ \tilde{Q} & \tilde{R}\end{bmatrix}\begin{Bmatrix}\nabla^2\hat{\varphi}_\mathrm{s}\\ \nabla^2\hat{\varphi}_\mathrm{f}\end{Bmatrix} = \begin{bmatrix}M_{11} & M_{12}\\ M_{12} & M_{22}\end{bmatrix}\begin{Bmatrix}\hat{\varphi}_\mathrm{s}\\ \hat{\varphi}_\mathrm{f}\end{Bmatrix} \tag{14}$$

With straight forward matrix inversion and multiplication, Eq. (14) can be expressed as

$$\begin{Bmatrix}\nabla^2\hat{\varphi}_\mathrm{s}\\ \nabla^2\hat{\varphi}_\mathrm{f}\end{Bmatrix} = \frac{1}{\Delta}\begin{bmatrix}\tilde{R}M_{11} - \tilde{Q}M_{12} & \tilde{R}, M_{12} - \tilde{Q}M_{22}\\ -\tilde{Q}M_{11} + (\tilde{\lambda}+2\mu)M_{12} & -\tilde{Q}M_{12} + (\tilde{\lambda}+2\mu)M_{22}\end{bmatrix}\begin{Bmatrix}\hat{\varphi}_\mathrm{s}\\ \hat{\varphi}_\mathrm{f}\end{Bmatrix} \tag{15}$$

in which $\Delta = (\tilde{\lambda}+2\mu)\tilde{R} - \tilde{Q}^2$. Solution of the system of the two simultaneous partial differential equations represented by Eq. (15) can be achieved elegantly by utilization of the Diagonalization technique

(Kreyszig, 1999). This technique entails the transformation of an n × n matrix into a diagonal matrix whose entries on the main diagonal are the eigenvalues of the original matrix. By use of vector notation, Eq. (15) can be presented as

$$\nabla^2\hat{\boldsymbol{\varphi}} = \mathbf{A}\hat{\boldsymbol{\phi}} \tag{16}$$

in which

$$\mathbf{A} = \begin{bmatrix} a_{11} & a_{12} \\ a_{21} & a_{22} \end{bmatrix}$$

where a_{ij} are the coefficients of the matrix in Eq. (15). Let

$$\boldsymbol{\varphi} = \mathbf{X}\mathbf{y} \tag{17}$$

in which $\mathbf{X}$ is a matrix of the eigenvectors of $\mathbf{A}$ with the coefficients

$$\begin{aligned} x_{11} &= \mathrm{x}_{12} = -a_{12} \\ x_{21} &= \frac{1}{2}a_{11} - \frac{1}{2}a_{22} + \frac{1}{2}\sqrt{a_{11}^2 - 2a_{11}a_{22} + a_{22}^2 + 4a_{12}a_{21}} \\ x_{22} &= \frac{1}{2}a_{11} - \frac{1}{2}a_{22} - \frac{1}{2}\sqrt{a_{11}^2 - 2a_{11}a_{22} + a_{22}^2 + 4a_{12}a_{21}} \end{aligned} \tag{18}$$

Then Eq. (16) becomes

$$\nabla^2\hat{\boldsymbol{\varphi}} = \mathbf{X}\nabla^2\hat{\mathbf{y}} = \mathbf{A}\hat{\boldsymbol{\varphi}} = \mathbf{A}\mathbf{X}\hat{\mathbf{y}} \tag{19}$$

Multiplying the second and the fourth term by $\mathbf{X}^{-1}$ from the left and noting that $\mathbf{X}^{-1}\mathbf{X} = \mathbf{I}$ (in which $\mathbf{I}$ is a unit matrix), Eq. (19) can be expressed as

$$\nabla^2\hat{\mathbf{y}} = \mathbf{X}^{-1}\mathbf{A}\mathbf{X}\hat{\mathbf{y}} = \mathbf{D}\hat{\mathbf{y}} \tag{20}$$

in which $\mathbf{D}$ is a diagonal matrix with the coefficients

$$\begin{aligned} D_{11} &= \zeta_{\mathrm{s}}^2 = \frac{1}{2}a_{11} + \frac{1}{2}a_{22} + \frac{1}{2}\sqrt{a_{11}^2 - 2a_{11}a_{22} + a_{22}^2 + 4a_{12}a_{21}} \\ D_{12} &= D_{21} = 0, \\ D_{22} &= \zeta_{\mathrm{f}}^2 = \frac{1}{2}a_{11} + \frac{1}{2}a_{22} - \frac{1}{2}\sqrt{a_{11}^2 - 2a_{11}a_{22} + a_{22}^2 + 4a_{12}a_{21}} \end{aligned} \tag{21}$$

where ζ_i^2 are used in stead of D_{ii} for convenience of notation. Thus Eq. (20) can be written in terms of uncoupled equations as

$$\nabla^2\hat{y}_1 - \zeta_1^2\hat{y}_1 = 0 \tag{22a}$$

$$\nabla^2\hat{y}_2 - \zeta_2^2\hat{y}_2 = 0 \tag{22b}$$

Solution of $\hat{y}_1$ and $\hat{y}_2$ may take the form

$$\begin{aligned} \hat{y}_1(r,z) &= \hat{y}_1(z)J_0(\xi r) \\ \hat{y}_2(r,z) &= \hat{y}_2(z)J_0(\xi r) \end{aligned} \tag{23}$$

in which J_0 is the Bessel function of the first kind of order 0. Substituting Eq. (23) into Eqs. (22a) and (22b) and solving the resulting ordinary differential equations yields

$$\begin{aligned}\hat{y}_1(r,z) &= B\mathrm{e}^{-\zeta_{\mathrm{ps}}z}J_0(\xi r)\\ \hat{y}_2(r,z) &= C\mathrm{e}^{-\zeta_{\mathrm{pf}}z}J_0(\xi r)\end{aligned} \tag{24}$$

in which $\zeta_{\mathrm{ps}} = \sqrt{\zeta_{\mathrm{s}}^2 + \xi^2}$ and $\zeta_{\mathrm{pf}} = \sqrt{\zeta_{\mathrm{f}}^2 + \xi^2}$ represent wavenumbers in the z-direction and the subscript p_i refers to the P-wave (dilatational wave) in the solid, $i = \mathrm{s}$, and the fluid $i = \mathrm{f}$. The constants of integration B and C are determined from the boundary conditions. As for Eq. (12), the second solutions of Eq. (24) have been discarded. Substitution of Eq. (24) into Eq. (17) yields the solution for the dilatational waves in solid and fluid as

$$\begin{aligned}\hat{\varphi}_{\mathrm{s}} &= -(Ba_{12}\mathrm{e}^{-\zeta_{\mathrm{ps}}z} + Ca_{12}\mathrm{e}^{-\zeta_{\mathrm{pf}}z})J_0(\xi r)\\ \hat{\varphi}_{\mathrm{f}} &= (Bx_{21}\mathrm{e}^{-\zeta_{\mathrm{ps}}z} + Cx_{22}\mathrm{e}^{-\zeta_{\mathrm{pf}}z})J_0(\xi r)\end{aligned} \tag{25}$$

In the limit case of dry soil, $\rho_{12} = \rho_{22} = 0$, $b = 0$, $R = Q \to 0$, and $\rho_{11} = \rho$, Eqs. (15) and (16) reduce to

$$\lim_{R,Q\to 0}\begin{Bmatrix}\nabla^2\hat{\varphi}_{\mathrm{s}}\\ \nabla^2\hat{\varphi}_{\mathrm{f}}\end{Bmatrix} = \lim_{R,Q\to 0}\left(\begin{bmatrix}a_{11} & a_{12}\\ a_{21} & a_{22}\end{bmatrix}\begin{Bmatrix}\hat{\varphi}_{\mathrm{s}}\\ \hat{\varphi}_{\mathrm{f}}\end{Bmatrix} = \frac{1}{(\tilde{\lambda}+2\mu)R - Q^2}\begin{bmatrix}RM_{11} & 0\\ -QM_{11} & 0\end{bmatrix}\begin{Bmatrix}\hat{\varphi}_{\mathrm{s}}\\ \hat{\varphi}_{\mathrm{f}}\end{Bmatrix}\right) \tag{26}$$

Then by dividing all terms in a_{11} by R and all terms in a_{21} by Q, in the limit case, they reduce to

$$\begin{aligned}&\lim_{R,Q\to 0} a_{11} = \frac{M_{11}}{\lambda+2\mu} = \frac{-\omega^2}{c_{\mathrm{p}}^2}\\ &\lim_{R,Q\to 0} a_{21} = 0\\ &a_{12} = a_{22} = 0\end{aligned} \tag{27}$$

Substituting Eq. (27) into Eqs. (18) and (21) yields,

$$\begin{aligned}D_{11} &= \zeta_{\mathrm{s}}^2 = a_{11} = x_{21}\\ D_{22} &= \zeta_{\mathrm{f}}^2 = 0 = x_{11} = x_{12} = x_{22}\end{aligned} \tag{28}$$

and by substituting Eqs. (27) and (28) into Eq. (25), the two equations for dilatational motions in solid and fluid reduce to a one equation of a dilatation motion in the dry solid as

$$\hat{\varphi}_{\mathrm{s}} = \hat{\varphi}_{\mathrm{f}} = \hat{\varphi} = A\mathrm{e}^{-\zeta_{\mathrm{p}}z}J_0(\xi r) \tag{29}$$

in which

$$\zeta_{\mathrm{p}} = \zeta_{\mathrm{ps}} = \sqrt{\zeta_{\mathrm{s}}^2 + \xi^2} = \sqrt{a_{11} + \xi^2} = \sqrt{-\frac{\omega^2}{c_{\mathrm{p}}^2} + \xi^2}$$

identical to that of the dry case (Al-Khoury et al., 2001a,b).

3. Formulation of a porous semi-infinite spectral element

The spectral element method (Doyle, 1997) is utilized for the formulation of an axi-symmetric semi-infinite spectral element for a porous medium. The element can be pictorially presented as shown in Fig. 1. As in the finite element method, the spectral element is defined by a stiffness matrix. However, the significance difference is that the inertia of the distributed mass is described exactly. As a consequence, one spectrally formulated element is sufficient to describe a whole layer without the need for subdivisions.

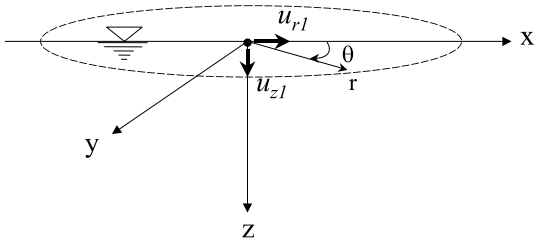

Fig. 1. Poroelastic semi-infinite spectral element.

For an axi-symmetric system the displacements can be obtained as

$$\begin{aligned}\hat{u}_r^i &= \frac{\partial\hat{\varphi}_i}{\partial r} - \frac{\partial\hat{\psi}_i}{\partial z}\\ \hat{u}_z^i &= \frac{\partial\hat{\varphi}_i}{\partial z} + \frac{1}{r}\frac{\partial(r\hat{\psi}_i)}{\partial r}\end{aligned} \tag{30}$$

in which $i = \mathrm{s}$ is for the solid phase and $i = \mathrm{f}$ is for the fluid phase. Substituting Eqs. (13) and (25) into Eq. (30) leads, for the solid phase, to

$$\begin{aligned}\hat{u}_r^{\mathrm{s}} &= \left(B\xi a_{12}\mathrm{e}^{-\zeta_{\mathrm{ps}}z} + C\xi a_{12}\mathrm{e}^{-\zeta_{\mathrm{pf}}z} + A\zeta_{\mathrm{sh}}\mathrm{e}^{-\zeta_{\mathrm{sh}}z}\right)J_1(\xi r)\\ \hat{u}_z^{\mathrm{s}} &= \left(B\zeta_{\mathrm{ps}}a_{12}\mathrm{e}^{-\zeta_{\mathrm{ps}}z} + C\zeta_{\mathrm{pf}}a_{12}\mathrm{e}^{-\zeta_{\mathrm{pf}}z} + A\xi\mathrm{e}^{-\zeta_{\mathrm{sh}}z}\right)J_0(\xi r)\end{aligned} \tag{31}$$

and for the fluid phase to

$$\begin{aligned}\hat{u}_r^{\mathrm{f}} &= -\left(B\xi x_{21}\mathrm{e}^{-\zeta_{\mathrm{ps}}z} + C\xi x_{22}\mathrm{e}^{-\zeta_{\mathrm{pf}}z} + A\frac{M_{12}}{M_{22}}\zeta_{\mathrm{sh}}\mathrm{e}^{-\zeta_{\mathrm{sh}}z}\right)J_1(\xi r)\\ \hat{u}_z^{\mathrm{f}} &= -\left(B\zeta_{\mathrm{ps}}x_{21}\mathrm{e}^{-\zeta_{\mathrm{ps}}z} + C\zeta_{\mathrm{pf}}x_{22}\mathrm{e}^{-\zeta_{\mathrm{pf}}z} + A\frac{M_{12}}{M_{22}}\xi\mathrm{e}^{-\zeta_{\mathrm{sh}}z}\right)J_0(\xi r)\end{aligned} \tag{32}$$

The relevant stresses can be obtained by substituting Eqs. (31) and (32) into Eq. (3), and knowing that the normal stress in Eq. (3) can be expressed as

$$\sigma_{zz} = 2\mu e_{zz} + \lambda e + \frac{\tilde{Q}}{\tilde{R}}\sigma \tag{33}$$

the normal stress for the solid phase is then

$$\begin{aligned}\hat{\sigma}_{zz} &= -\left(2A\mu\zeta_{\mathrm{sh}}\xi\mathrm{e}^{-\zeta_{\mathrm{sh}}z} + Ba_{12}\mathrm{e}^{-\zeta_{\mathrm{ps}}z}\left\{(\lambda+2\mu)\zeta_{\mathrm{p1}}^2 - \lambda\xi^2\right\} + Ca_{12}\mathrm{e}^{-\zeta_{\mathrm{pf}}z}\left\{(\lambda+2\mu)\zeta_{\mathrm{pf}}^2 - \lambda\xi^2\right\}\right)J_0(\xi r) + \frac{\tilde{Q}}{\tilde{R}}\hat{\sigma}\\ \hat{\tau}_{zr} &= -\mu\left(A\mathrm{e}^{-\zeta_{\mathrm{sh}}z}\left(\zeta_{\mathrm{sh}}^2 + \xi^2\right) + 2Ba_{12}\xi\zeta_{\mathrm{ps}}\mathrm{e}^{-\zeta_{\mathrm{ps}}z} + 2Ca_{12}\xi\zeta_{\mathrm{pf}}\mathrm{e}^{-\zeta_{\mathrm{pf}}z}\right)J_1(\xi r)\end{aligned} \tag{34}$$

and for the fluid phase is

$$\begin{aligned}\hat{\sigma} = -\Big(&\tilde{Q}a_{12}\left\{B\mathrm{e}^{-\zeta_{\mathrm{ps}}z}\left(\xi^2 - \zeta_{\mathrm{ps}}^2\right) + C\mathrm{e}^{-\zeta_{\mathrm{pf}}z}\left(\xi^2 - \zeta_{\mathrm{pf}}^2\right)\right\}\\ &- \tilde{R}\left\{Bx_{21}\mathrm{e}^{-\zeta_{\mathrm{ps}}z}\left(\xi^2 - \zeta_{\mathrm{ps}}^2\right) + Cx_{22}\mathrm{e}^{-\zeta_{\mathrm{pf}}z}\left(\xi^2 - \zeta_{\mathrm{pf}}^2\right)\right\}\Big)J_0(\xi r)\end{aligned} \tag{35}$$

If a drained condition exists at the surface $z = 0$ or at the contact surface with a dry layer, which is normally the case in practice, no excess pore pressure can be developed such that

$$\hat{\sigma} = -\phi p = 0 \tag{36}$$

Substituting Eq. (36) into Eq. (35), a relationship between B and C can be established as

$$C = -\Xi B \tag{37}$$

in which

$$\Xi = \frac{\tilde{Q}a_{12}(\xi^2 - \zeta_{\mathrm{ps}}^2) + \tilde{R}x_{21}(\xi^2 - \zeta_{\mathrm{pf}}^2)}{\tilde{Q}a_{12}(\xi^2 - \zeta_{\mathrm{pf}}^2) + \tilde{R}x_{22}(\xi^2 - \zeta_{\mathrm{pf}}^2)}$$

where a_{ij} and x_{ij} are as defined in Eqs. (16) and (18) respectively. By substituting Eq. (37) into Eqs. (31), (32) and (34) the displacements and stresses can be determined in terms of only two constants A and B. These constants can be quantified by solving for the boundary conditions at the element node. Let the radial and vertical displacements of the skeleton at the node, $z = 0$, be equal to u_{r1}^{s} and u_{z1}^{s} respectively, Fig. 1. The displacements, in the z coordinate, at the node becomes

$$\begin{aligned} \hat{u}_{r1}^{\mathrm{s}} &= A\zeta_{\mathrm{sh}} + Ba_{12}\xi(1 - \Xi) \\ \hat{u}_{z1}^{\mathrm{f}} &= A\xi + Ba_{12}(\zeta_{\mathrm{ps}} - \Xi\zeta_{\mathrm{pf}}) \end{aligned} \tag{38}$$

Solution of Eq. (38) in terms of A and B leads to

$$\begin{Bmatrix} A \\ B \end{Bmatrix} = \frac{1}{\Delta}\begin{bmatrix} -\xi/a_{12} & \zeta_{\mathrm{sh}}/a_{12} \\ -\zeta_{\mathrm{ps}} + \Xi\zeta_{\mathrm{pf}} & -\xi(1 - \Xi) \end{bmatrix}\begin{Bmatrix} \hat{u}_{r1}^{\mathrm{s}} \\ \hat{u}_{z1}^{\mathrm{s}} \end{Bmatrix} \tag{39}$$

in which

$$\Delta = -\xi^2(1 - \Xi) + \zeta_{\mathrm{sh}}(\zeta_{\mathrm{ps}} - \Xi\zeta_{\mathrm{pf}})$$

As for the displacements, the stresses at the node ($z = 0$) can be expressed by means of Eq. (37) as

$$\begin{aligned} \hat{\sigma}_{zz1} &= -\Big(2A\mu\xi\zeta_{\mathrm{sh}} + Ba_{12}\Big\{(\lambda + 2\mu)\zeta_{\mathrm{ps}}^2 - \lambda\xi^2 - \Xi\Big\{(\lambda + 2\mu)\zeta_{\mathrm{pf}}^2 - \lambda\xi^2\Big\}\Big\}\Big) \\ \hat{\tau}_{zr1} &= -\mu\big(A\big(\zeta_{\mathrm{sh}}^2 + \xi^2\big) + 2Ba_{12}\xi\big(\zeta_{\mathrm{ps}} - \Xi\zeta_{\mathrm{pf}}\big)\big) \end{aligned} \tag{40}$$

Following the Cauchy stress principle, the tractions at node 1 are related to the stresses by

$$\hat{T}_{z1} = -\hat{\sigma}_{zz1} \text{ and } \hat{T}_{r1} = -\hat{\tau}_{zr1} \tag{41}$$

On substituting Eq. (40) into Eq. (41), the following relationships are obtained between the applied traction $\hat{T}_{z1}$ and $\hat{T}_{r1}$ and the constants A and B as

$$\begin{Bmatrix} \hat{T}_{z1} \\ \hat{T}_{r1} \end{Bmatrix} = \begin{bmatrix} 2\mu\xi\zeta_{\mathrm{sh}} & a_{12}\Big\{(\lambda + 2\mu)\zeta_{\mathrm{ps}}^2 - \lambda\xi^2 - \Xi\Big\{(\lambda + 2\mu)\zeta_{\mathrm{pf}}^2 - \lambda\xi^2\Big\}\Big\} \\ \mu\big(\zeta_{\mathrm{sh}}^2 + \xi^2\big) & 2\mu a_{12}\xi\big(\zeta_{\mathrm{ps}} - \Xi\zeta_{\mathrm{pf}}\big) \end{bmatrix}\begin{Bmatrix} A \\ B \end{Bmatrix} \tag{42}$$

Upon substituting the vector $\{AB\}^{\mathrm{T}}$ of Eq. (39) into Eq. (42), a relationship is obtained between the applied traction and the displacements at the node that can symbolically be expressed as

$$\hat{\mathbf{T}} = \hat{\mathbf{k}}\hat{\mathbf{u}} \tag{43}$$

in which $\hat{\mathbf{k}}$ represents the stiffness matrix of the spectral semi-infinite element in resemblance to that of the finite element. The stiffness matrix for the half space porous medium is complex and non-symmetric 2×2 matrix with coefficients

$$\begin{aligned}
\hat{k}_{11} &= \frac{1}{\Delta}\Big(-\xi\Big\{(\lambda+2\mu)\zeta_{ps}^2 - \lambda\xi^2 - \Xi\Big\{(\lambda+2\mu)\zeta_{pf}^2 - \lambda\xi^2\Big\}\Big\} + 2\mu\xi\zeta_{sh}\big(\zeta_{ps} - \Xi\zeta_{pf}\big)\Big)\\
\hat{k}_{12} &= \frac{1}{\Delta}\Big(\zeta_{sh}\Big\{(\lambda+2\mu)\zeta_{ps}^2 - \lambda\xi^2 - \Xi\Big\{(\lambda+2\mu)\zeta_{pf}^2 - \lambda\xi^2\Big\}\Big\} - 2\mu\xi^2\zeta_{sh}(1-\Xi)\Big)\\
\hat{k}_{21} &= \frac{1}{\Delta}\big(-2\mu\xi^2\big(\zeta_{ps} - \Xi\zeta_{pf}\big) - \mu\big(\zeta_{sh}^2 + \xi^2\big)\big(-\zeta_{ps} + \Xi\zeta_{pf}\big)\big)\\
\hat{k}_{22} &= \frac{1}{\Delta}\big(2\mu\xi\zeta_{sh}\big(\zeta_{ps} - \Xi\zeta_{pf}\big) - \mu\xi\big(\zeta_{sh}^2 + \xi^2\big)(1+\Xi)\big)
\end{aligned} \tag{44}$$

in which Δ is as defined in Eq. (39). The non-symmetry of the stiffness matrix is due to the imposition of a drained condition at the element surface. The imposition of this condition has resulted to an element with only two degrees of freedom at the node similar to that of the single phase elements developed earlier (Al-Khoury et al., 2001a,b).

4. The boundary value problem

A general solution of the system of equations, Eq. (43), is obtained by solving for the boundary conditions. The spectral element developed in the previous section can be utilized for solving general boundary value problems suitable for either finite or infinite homogeneous boundary conditions. As stated earlier, the objective of this research work is the development of a forward model capable of describing wave propagation in a pavement structure generated by the load impact of a FWD. As such, wave phenomena within a finite region from the load center are of interest. This implies that a homogeneous boundary at $r = R$ is postulated such that

$$\hat{u}(r, z = \text{cnt}) = 0, \quad r = R \tag{45a}$$

in which R is some distance, far from the source, at which waves are known a priori to vanish. It may be argued that imposing zero displacement at distance R does not account for the radiation of waves at infinity. However, waves in an axi-symmetric system would have a Bessel function representation, Eqs. (13) and (25). This function has the appropriate radiation behavior at large distance R. As long as R is large enough, the finite space window effectively approximates an infinite window. This is precisely what is done when time domain reconstruction is typically achieved by using the discrete Fourier transform (DFT) or the fast Fourier transform (FFT).

At the element surface, $z = 0$, a normal traction and/or a shear traction can be applied as

$$\left.\begin{aligned}
\hat{T}_z(r, z=0) &= \begin{cases} S(r), & 0 \leqslant r \leqslant a \\ 0, & a < r \leqslant R \end{cases}\\
\hat{T}_r(r, z=0) &= \begin{cases} D(r), & 0 \leqslant r \leqslant a \\ 0, & a < r \leqslant R \end{cases}
\end{aligned}\right\} \tag{45b}$$

in which a is the radius of the applied traction.

The imposition of the condition of Eq. (45a) to Eq. (31) yields, symbolically,

$$\hat{u}(R, z = \text{cnt}) = \hat{Z}(z = \text{cnt})\hat{R}(R) = 0 \tag{46}$$

in which $\hat{Z}(z = \text{cnt})$ is the function between brackets in Eq. (31) and $\hat{R}(R)$ is the Bessel function. The non-trivial solution of Eq. (46), for a given z, and in reference to Eq. (31), is

$$\hat{R}(R) = J_v(\xi R) = 0 \tag{47}$$

This condition can be satisfied at the infinitely many positive roots α_m of the J_v function (Abramowitz and Stegun, 1972). Eq. (47) implies $\xi R = \alpha_m$, thus $\xi = \xi_m = \alpha_m/R$. Hence the m functions

$$\hat{R}_m(r) = J_v(\xi_m r) = J_v\left(\frac{\alpha_m}{R} r\right) \tag{48}$$

are solutions to the wave equations, Eq. (4), in the radial direction, with each m corresponding to the mth normal mode of vibration. It can be noticed here that the homogenous boundary condition at $r = R$ has inevitably lead to an a-priori known discrete set of normal modes of vibration. This discretization is applicable to all points within the region z, $r < R$. It is this choice that renders this technique computationally attractive over those, which involve discretization of physical systems with infinite boundaries. In the later, ξ_m has to be evaluated numerically for each output point. Such evaluation is computationally difficult due to the semi-infinite upper limit of the inverse wave number integral, Eq. (1), the oscillatory nature of the Bessel function and the presence of surface wave poles of the integrand. These exacerbate at points relatively far from the source, causing numerical instabilities.

It follows that the general solution of Eq. (31) that satisfies the homogenous condition $\hat{\boldsymbol{u}}(R,z) = 0$ can be presented by the series

$$\begin{aligned}
\hat{u}_r^{\mathrm{s}} &= \sum_{m=1}^{\infty} \left(B_m \xi_m a_{12} \mathrm{e}^{-\zeta_{\mathrm{ps}m} z} + C_m \xi_m a_{12} \mathrm{e}^{-\zeta_{\mathrm{pf}m} z} + A_m \zeta_{\mathrm{sh}m} \mathrm{e}^{-\zeta_{\mathrm{sh}m} z}\right) J_1(\xi_m r) \\
\hat{u}_z^{\mathrm{s}} &= \sum_{m=1}^{\infty} \left(B_m \zeta_{\mathrm{ps}m} a_{12} \mathrm{e}^{-\zeta_{\mathrm{ps}m} z} + C_m \zeta_{\mathrm{pf}m} a_{12} \mathrm{e}^{-\zeta_{\mathrm{pf}m} z} + A_m \xi_m \mathrm{e}^{-\zeta_{\mathrm{sh}m} z}\right) J_0(\xi_m r)
\end{aligned} \tag{49}$$

in which C_m is as defined in Eq. (37). Same is applicable to the fluid displacements, Eq. (32).

These functions, $\hat{u}_r^{\mathrm{s}}$ and $\hat{u}_z^{\mathrm{s}}$, are the eigenfunctions of the vibrating system and the values $\xi_m = \alpha_m/R$ are their corresponding eigenvalues. Basically a series of these eigenfunctions for infinitely many eigenvalues ($m = 1 \to \infty$) should be able to simulate wave propagation in the system for the chosen boundary conditions. However, as it will be shown later, summation over limited number of eigenvalues ($m = 1 \to M$) will suffice.

It follows that the general solutions to the stress functions, Eqs. (34) and (35), are also described by a series summation over m eigenvalues. Thus, at the element surface, $z = 0$, the general solution to Eq. (40) yields

$$\begin{aligned}
\hat{\sigma}_{zz1} &= \sum_{m=1}^{\infty} - \left(2A_m \mu \xi_m \zeta_{\mathrm{sh}m} + B_m a_{12} \left\{(\lambda + 2\mu)\zeta_{\mathrm{ps}m}^2 - \lambda \xi_m^2 - \Xi\left\{(\lambda + 2\mu)\zeta_{\mathrm{pf}m}^2 - \lambda \xi_m^2\right\}\right\}\right) J_0(\xi_m r) \\
\hat{\tau}_{zr1} &= \sum_{m=1}^{\infty} - \mu\left(A_m\left(\zeta_{\mathrm{sh}m}^2 + \xi_m^2\right) + 2B_m a_{12} \xi_m \left(\zeta_{\mathrm{ps}m} - \Xi \zeta_{\mathrm{pf}m}\right)\right) J_1(\xi_m r)
\end{aligned} \tag{50}$$

Applying the boundary conditions in Eq. (45b) to Eq. (50), and by means of Eq. (41), the surface traction, in the region $0 \leqslant r \leqslant a$, can be described as

$$\hat{T}_{z1} = -\hat{\sigma}_{zz1} = \sum_{m=1}^{\infty} - \hat{F}_{zm} J_0(\xi_m r) = S(r) \tag{51a}$$

$$\hat{T}_{r1} = -\hat{\tau}_{rz1} = \sum_{m=1}^{\infty} - \hat{F}_{rm} J_1(\xi_m r) = D(r) \tag{51b}$$

in which $\hat{F}_{im} (= \hat{F}_{zm}$ or $\hat{F}_{rm})$ represents the terms between brackets in Eq. (50). Eqs. (51a) and (51b) is a typical form of a Fourier–Bessel series with coefficient $\hat{F}_{im}$, which can be determined analytically (Kreyszig, 1999) as

$$\hat{F}_{im} = \frac{2}{R^2 J_{v+1}^2(\alpha_m)} \int_0^R r g(r) J_v(\xi_m r)\,\mathrm{d}r \tag{52}$$

where $g(r)$ represents either $S(r)$ or $D(r)$ in Eq. (50). Substituting Eqs. (51a) and (51b) into Eq. (42) leads, for the m eigenvalue, to

$$\begin{Bmatrix} \hat{F}_{zm} \\ \hat{F}_{rm} \end{Bmatrix} = \begin{bmatrix} 2\mu\xi_m\zeta_{\mathrm{sh}m} & a_{12}\Big\{(\lambda+2\mu)\zeta_{\mathrm{ps}m}^2 - \lambda\xi_m^2 - \Xi\Big\{(\lambda+2\mu)\zeta_{\mathrm{pf}m}^2 - \lambda\xi_m^2\Big\}\Big\} \\ \mu\big(\zeta_{\mathrm{sh}m}^2 + \xi_m^2\big) & 2\mu a_{12}\xi_m\big(\zeta_{\mathrm{ps}m} - \Xi\zeta_{\mathrm{pf}m}\big) \end{bmatrix} \begin{Bmatrix} A_m \\ B_m \end{Bmatrix} \tag{53}$$

in which

$$\begin{Bmatrix} A_m \\ B_m \end{Bmatrix} = \frac{1}{\Delta} \begin{bmatrix} -\xi_m/a_{12} & \zeta_{\mathrm{sh}m}/a_{12} \\ -\zeta_{\mathrm{ps}m} + \Xi\zeta_{\mathrm{pf}m} & -\xi_m(1-\Xi) \end{bmatrix} \begin{Bmatrix} \hat{u}_{r1}^{\mathrm{s}} \\ \hat{u}_{z1}^{\mathrm{s}} \end{Bmatrix} \tag{54}$$

where $\Delta = -\xi_m^2(1-\Xi) + \zeta_{\mathrm{sh}m}(\zeta_{\mathrm{ps}m} - \Xi\zeta_{\mathrm{pf}m})$.

Substituting Eq. (54) into Eq. (53) and solving the resulting system of equations give the displacements at the element node. By substituting back these displacements into Eq. (54) gives A_m and B_m. Once these constants are quantified, then, by substituting them into Eqs. (31) and (32), the displacements at any point in the half space can be determined. Also, by substituting these constants into Eqs. (34) and (35) the stresses and excess pore pressure at any point can be obtained. This applies to the case of a layered structure where Eq. (43) becomes $\hat{\mathbf{T}} = \hat{\mathbf{K}}\hat{\mathbf{U}}$, in which $\hat{\mathbf{K}}$ is the global stiffness matrix and $\hat{\mathbf{U}}$ is the structural degrees-of-freedom vector.

5. Element verification

The porous media spectral element has been implemented in the spectral element code layered media dynamic analysis (LAMDA), (Al-Khoury et al., 2001a,b). Verification of the newly developed element has been done by comparing the response of a multi-layer system consisting of dry and fully saturated layers with that obtained from the finite element method. The finite element system INSAP-PM (Liu et al., 2000) was utilized for this purpose.

In an earlier publication (Al-Khoury et al., 2001a,b) two axi-symmetric spectral elements (a layer element and a semi-infinite element) for a one-phase medium were developed. The layer element can be pictorially presented as in Fig. 2. In the vertical direction it extends to $z = h$ and in the horizontal direction

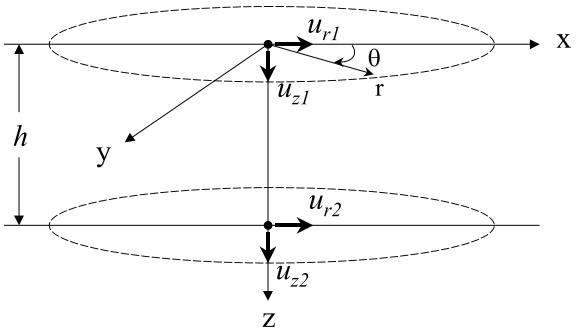

Fig. 2. One-phase axi-symmetric layer element (Al-Khoury et al., 2001a,b).

it extends to the $r = R$, where the wave motion vanishes. The element is physically defined by two nodes each having one radial and one vertical degree of freedom.

As stated earlier, the drain condition imposed at the surface of the semi-infinite porous spectral element has lead to solving for only two degrees of freedom at the node. This enables direct assemblage with the previously derived one-phase elements. A multi-layer system consisting of dry layers and a saturated half space can thus be simulated.

Assemblage of spectral structural stiffness matrix follows the same procedures as that of the conventional finite element method but the assemblage is done for every frequency ω_n and wavenumber ξ_m. Both embedded and/or surface loads can be applied. Here, a uniformly distributed normal force applied on a circular area at the surface of a layered system will be simulated for verification of element derivation and computer implementation.

A layered medium representing a typical pavement structure subjected to a FWD load pulse was simulated. The structure was assumed to consist of three layers; asphalt (E modulus = 1000 MPa and $h = 150$ mm), subbase (E modulus = 200 MPa and $h = 250$ mm) and a fully saturated subgrade (E modulus = 25 MPa and $h = \propto$ mm). Poisson's ratio for all materials is 0.35. The material parameters for the porous media were assumed as follows:

$$\rho_s = 1500 \text{ kg/m}^3, \quad \rho_f = 1000 \text{ kg/m}^3, \quad \kappa = 0.0001 \text{ mm/s}, \quad \phi = 0.8, \quad \beta = 0.97, \quad \tilde{M} = 1200 \text{ MPa}$$

The tortuosity parameter proposed by Berryman and Thigpen (1985) $\tilde{a} = (1 + 1/\phi)/2$ was utilized. It is worth mentioning here that other researchers have assumed $\rho_{12} = 0$ (see description of parameters of Eq. (2)). During the development of this research work both formulations were examined and found that no difference can be observed, at least for the cases under investigation. Also, it was found that, for the cases and frequency spectrum under investigation, variations of the tortuosity parameter between 1 and 3 cause no observable differences in the response. Other researchers have come to same conclusion (see for example Halpern and Christiano, 1986; Bougacha et al., 1993).

In LAMDA, the geometry was simulated by the use of two one-phase layer elements and 1 semi-infinite porous element. The FWD load pulse was simulated as

$$P(r,t) = F(t)S(r) \tag{55}$$

where $F(t)$ is an arbitrary function of time and $S(r)$ is the spatial function of the load distribution in the radial direction. $F(t)$ was represented by a complex exponential Fourier series as

$$F(t) = \sum_{n=0}^{\infty} \hat{F}_n e^{i\omega_n t} \tag{56}$$

in which $\hat{F}_n$ is the nth Fourier coefficient. $\hat{F}_n$ can best be determined by means of the FFT (Brigham, 1988).

Typical time history of the FWD load pulse $F(t)$ and its frequency spectrum are shown in Fig. 3. The number of samples are $N = 2048$. It can be seen that, for such a load pulse, the force magnitudes at frequencies beyond 150 Hz are not significance. Hence, the analysis to a maximum frequency of 150 Hz, that is $n = 77$, will suffice.

On the other hand, the spatial function $S(r)$ that describes the spatial geometry of the FWD loading plate was presented, by means of Eq. (51a), as

$$S(r) = \frac{1}{A} \sum_{m=1}^{\infty} \hat{F}_m J_0(\xi_m r), \quad 0 \leqslant r \leqslant a \tag{57}$$

in which A is the surface area of the FWD loading plate with radius a and $\hat{F}_m (= \hat{F}_{zm})$ is the Fourier–Bessel coefficient. For a cylindrical shape load with radius a and a unit amplitude, the coefficient $\hat{F}_m$ can then be determined (Al-Khoury et al., 2001a,b) as

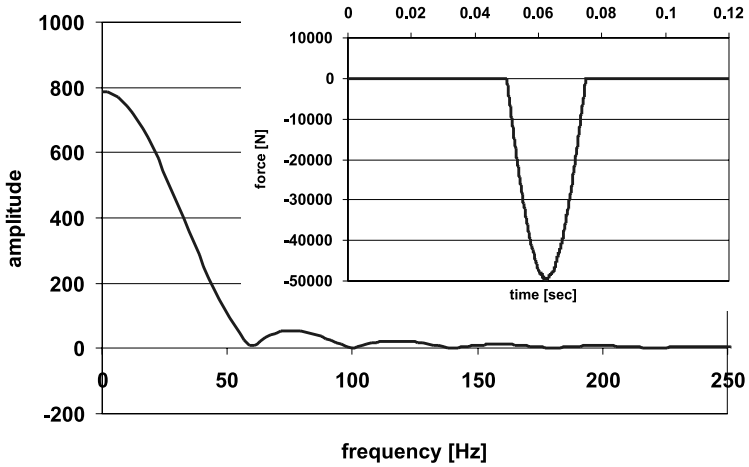

Fig. 3. FWD load pulse and its spectrum.

$$\hat{F}_m = \frac{2a}{\alpha_m R J_1^2(\alpha_m)} J_1\left(\frac{\alpha_m}{R} a\right) \tag{58}$$

$\hat{F}_m$ is an alternating function, which requires a relatively large number of samples. The number of samples necessary to describe the spatial geometry of the loading plate, for $a = 150$ mm and $R = 150$ mm, was $M = 1700$, which was obtained by experiment. The boundary distance $R = 150$ m was chosen, arbitrarily, to insure that no FWD induced waves can arrive.

Solution of the system of equations for determination of the displacements at the nodes is done by complex matrix inversion of the assembled stiffness matrix. The number of matrix inversions required, for this specific case, is $N \times M = 77 \times 1700$. Even though the number of matrix inversions seems to be large, the computation time is extremely short because of the small number of the system of equations involved in formulating the spectral element stiffness matrices.

In the finite element system INSAP-PM, the geometry was simulated by use of 1040, 20 noded brick elements. INSAP-PM is capable to simulate dry, partially saturated and fully saturated media under both static and dynamic loading conditions. The structure was assumed to extend 6 m in the horizontal direction and 15.4 m in the vertical direction. Also, because of symmetry, only a quadrant of the pavement was simulated. The radius of the loaded area was 150 mm. The detailed mesh surrounding the loaded area is shown in Fig. 4.

The oscillation of the pavement surface, at several locations, as computed by INSAP-PM is presented in Fig. 5(a) and by LAMDA in Fig. 5(b). It can be seen that the results are similar except that in the finite element analysis some disturbances appear at the end of the response, which can be attributed to the reflections at the boundaries of the mesh. The execution times were about 2 min for the spectral element method in an Intel 300 MHz PC, and about 1 h for the finite element method in a Digital Alpha 600 MHz Workstation.

6. Inverse calculation of layer parameters

In Al-Khoury et al. (2001a,b) details of the parameter identification procedure for layered systems were presented. The focus was on the interpretation of data obtained from the FWD test of pavement structures.

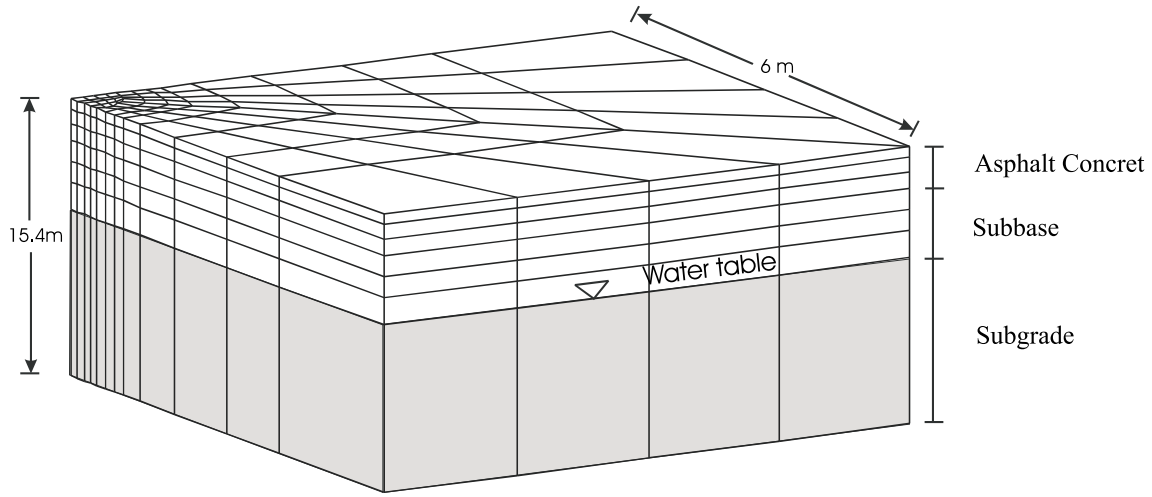

Fig. 4. INSAP-PM finite element mesh.

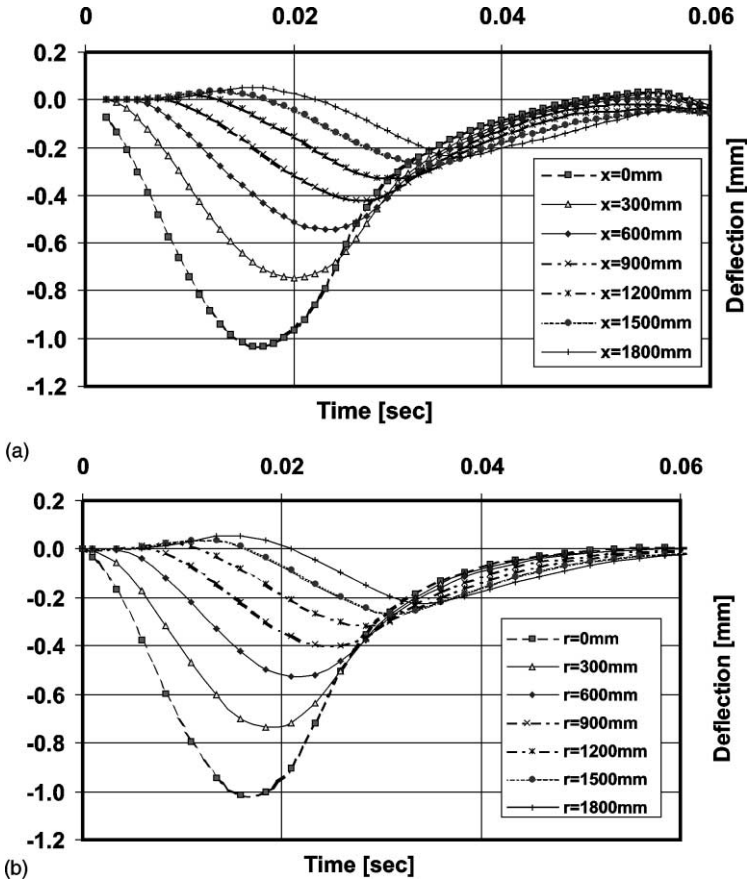

Fig. 5. Surface displacements (a) INSAP-PM, (b) LAMDA.

In the present contribution a brief review of the parameter identification procedure is presented. The emphasis has been placed on the application of the procedure for the determination of layer parameters in the presence of a saturated subgrade. The effect of ignoring the porous medium in the back calculation of layer parameters is examined.

In the proposed parameter identification technique of layered systems, the procedure begins with the estimation of system transfer functions from measured input/output data. On the basis of the formulations presented in the previous sections, the theoretical transfer functions are determined. Parameter identification is then performed by means of iterative solution of the system objective function, which describes the theoretical transfer functions in terms of the measured once.

The system objective function is presented as

$$q(\mathbf{x}) = \left| \sum_m \hat{F}_m \hat{G}(z, \xi_m, \omega_n) J_0(\xi_m l) \right|_{\text{theoretical}} - \left| \hat{G}_l(\omega_n) \right|_{\text{measured}} \leqslant \varepsilon \tag{59}$$

in which $\hat{G}(z, \xi_m, \omega_n)$ represents the theoretical transfer function at sensor location l, (obtained from the inversion of the assembled stiffness matrix), and $\hat{G}_l(\omega_n)$ represents its corresponding experimental transfer function. $\mathbf{x}$ in Eq. (59) represents the vector of the unknown variables such as layer elastic modulus, thickness, etc. and ε is a convergence criterion.

The solution of a system of multi-dimensional non-linear equations, such as Eq. (59), requires minimization techniques. In Al-Khoury et al. (2001a,b) three minimization algorithms (Factored Secant Update, Modified Levenberg–Marquardt and Modified Powell Hybrid) were utilized and examined in terms of their stability and rate of convergence. Here only the Modified Powell hybrid algorithm (Scales, 1985) for solving a non-constrained system of non-linear simultaneous equations with a finite-difference Jacobian was utilized.

6.1. Engineering application

Parameter identification of pavement layers is usually done by assuming dry profiles. However, roads, in many parts of the world, are built on water-saturated subgrades. As was shown earlier, due to the interaction between the solid particles and the fluid, waves of different nature exist in the wet profiles as compared with the dry ones (Biot, 1956). As a consequence, the use of dry models to simulate wet profiles may produce erroneous results.

To illustrate this, two forward analyses were conducted to simulate a pavement structure consisting of an asphalt layer (E modulus = 1000 MPa and $h = 150$ mm), a subbase layer (E modulus = 200 MPa and $h = 250$ mm) and a subgrade layer (E modulus = 10 MPa and $h = \propto$ mm). In one case, the subgrade was assumed dry and in the other it was assumed fully saturated. Surface responses, for both cases, are shown in Fig. 6. Comparing the two figures shows that the displacement magnitudes for the dry case are larger than those for the wet case. The reason for this is that in the wet case the development of the excess pore pressure contributes to the resistance to the applied forces and therefore less displacements are exhibited. Also, it can be noticed that in the case of wet profile, more uplifting occurs at the surface compared with that for the dry case.

The data obtained from the wet profile, Fig. 6a, were used as input to the inverse model to calculate back the original elastic moduli of the layer materials. Two forward models were utilized; one with one-phase elements (two layer elements and one semi-infinite element), and another consisting of two one-phase layer elements and a semi-infinite two-phase element. The results of the parameter identification algorithm are shown in Table 1. It can be seen that the use of the porous model enables accurate backcalculation of the material parameters. However, if a dry model is utilized, it will overestimate the material parameters.

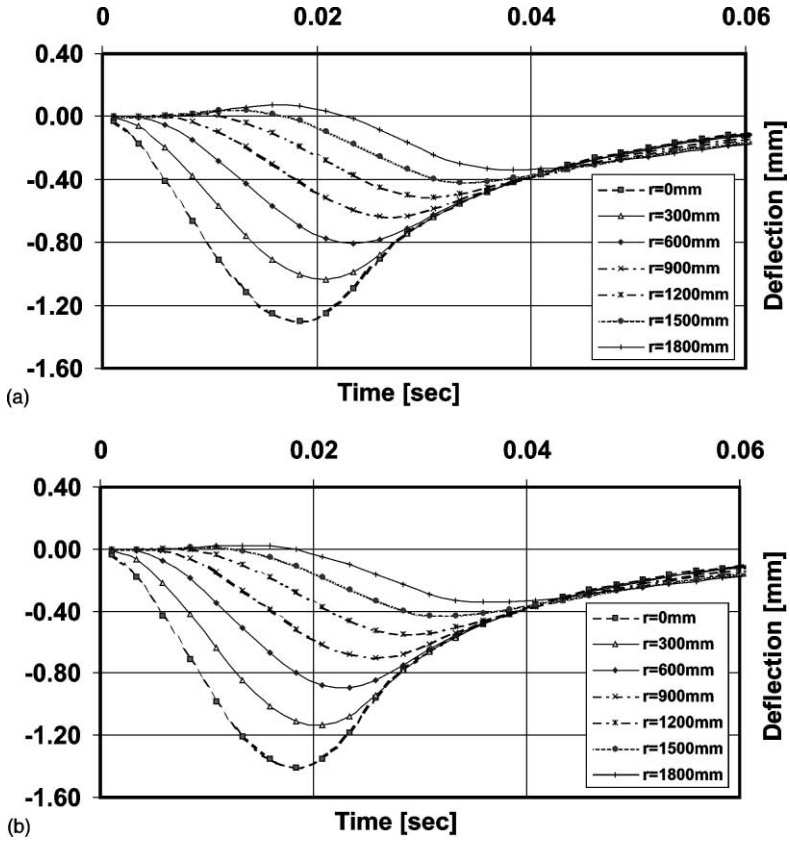

Fig. 6. Surface displacements (a) wet profile, (b) dry profile.

Table 1
Backcalculation by means of different forward models

Layer	Actual values (MPa)	Initial guess	Backcalculated	
			Dry case	Wet case
Asphalt	1000	200	1130	1000
Subbase	200	40	230	200
Subgrade	10	2	25	10

The inverse calculations were done for a single frequency. The number of iterations were about 15 iteration, each takes <2 s in an Intel 300 MHz PC.

7. Conclusions

The proposed methodology that combines Biot's theory of propagation of elastic waves in a fluid-saturated porous solid with the spectral element technique has been shown to be an efficient computational tool for analyzing the dynamic behavior of multi-layer systems consisting of both one- and two-phase

material layers. The advantages and the robustness of the proposed methodology can be attributed to the following reasons:

1. The spectral element method describes waves exactly, and hence, one element is adequate to describe a whole layer. Consequently, the size of the mesh of a layered system is only as large as the number of the layers involved.
2. The response of the developed two-phase element can be computed on the basis of the two displacement degrees of freedom, similar to that of the one-phase elements. This reduces the size of the system of equations, and also, enables direct assembly with the one-phase layer elements.
3. The spatial domain (in the radial direction) is considered to span to a "finite" boundary, where waves are postulated to vanish. Element formulation over such a domain has lead inevitably to series summation over discrete number of vibration modes. This avoids the inconvenience of the numerical evaluation of infinite integration involve in far field formulations.

Because of the computational efficiency, the methodology is suitable for direct utilization in iterative schemes for parameter identification of pavement layered systems on the basis of FWD measurements. It is shown that ignoring the presence of saturated subgrade may overestimate the backcalculated layer moduli.

References

Abramowitz, M., Stegun, I.A., 1972. Handbook of Mathematical Functions. Dover Publication, New York.

Achenbach, J.D., 1973. Wave propagation in elastic solids. North–Holland Publishing Company, Netherlands.

Al-Khoury, R., Scarpas, A., Kasbergen, C., Blaauwendraad, J., 2001a. Spectral element technique for efficient parameter identification of layered media. Part I. Forward calculation. International Journal of Solids and Structures 38, 1605–1623.

Al-Khoury, R., Kasbergen, C., Scarpas, A., Blaauwendraad, J., 2001b. Spectral element technique for efficient parameter identification of layered media. Part II. Inverse calculation. International Journal of Solids and Structures 38, 8753–8772.

Berryman, J.G., Thigpen, L., 1985. Linear dynamic poroelasticity with microstructure for partially saturated porous solids. Journal of Applied Mechanics 52, 345–350.

Biot, M.A., 1956. Theory of propagation of elastic waves in a fluid-saturated porous solid. I. Low-frequency range. Journal of the Acoustical Society of America 28, 168–178.

Biot, M.A., Willis, D.G., 1957. The elastic coefficients of the theory of consolidation. Journal of Applied Mechanics 24, 594–601.

Bougacha, S., Tassoulas, J., Roesset, J., 1993. Analysis of foundation on fluid-filled poroelastic stratum. Journal of Engineering Mechanics, ASCE 119, 1632–1648.

Bourbie, T., Coussy, O., Zinszner, B., 1987. Acoustics of Porous Media. Gulf Publishing Company.

Brigham, E.O., 1988. The Fast Fourier Transform and Its Applications. Prentice-Hall, Englewood Cliffs, NJ.

Degrande, G., De Roeck, G., 1992. A spectral element method for two-dimensional wave propagation in horizontally layered saturated porous media. Journal of Computers and Structures 44, 717–728.

Degrande, G., De Roeck, G., Van Den Broeck, P., Smeulders, D., 1998. Wave propagation in layered dry, saturated and unsaturated poroelastic media. International Journal of Solids and Structures 35, 4753–4778.

Doyle, J.F., 1997. Wave Propagation in Structures: Spectral Analysis Using Fast Discrete Fourier Transforms. Springer-Verlag, New York.

Halpern, M., Christiano, P., 1986. Response of poroelastic halfspace to steady-state harmonic surface tractions. International Journal for Numerical and Analytical Methods in Geomechanics 10, 609–632.

Kausel, E., Roesset, J.M., 1981. Stiffness matrices for layered soils. Bulletin of the Seismological Society of America 71, 1743–1761.

Khalili, N., Yazdchi, M., Valliappan, S., 1999. Wave propagation analysis of two-phase saturated porous media using coupled finite-infinite element method. International Journal of Soil Dynamics and Earthquake Engineering 18, 533–553.

Kreyszig, E., 1999. Advanced Engineering Mathematics. John Wiley & Sons, New York.

Liu, X., Scarpas, A., Blaauwendraad, J., 2000. Finite Element Investigation of the Influence of Saturated Subgrade on FWD Testing. In: Proceedings of the TRB2000 conference, Washington, DC.

Lysmer, J., 1970. Lumped mass method for Rayleigh waves. Bulletin of the Seismological Society of America 60, 89–104.

Philippacopoulos, A., 1988. Lamb's problem for fluid-saturated, porous media. Bulletin of the Seismological Society of America 78, 908–923.

Rizzi, S., Doyle, J., 1992. A spectral element approach to wave motion in layered solids. Journal of Vibration and Acoustics 114, 569–577.

Scales, L.E., 1985. Introduction to non-linear optimization. Macmillan.

Senjuntichai, T., Rajapakse, R.K., 1995. Exact stiffness method for quasi-statics of a multi-layered poroelastic medium. International Journal of Solids and Structures 32, 1535–1553.

Seale, S.H., Kausel, E., 1989. Point loads in cross-anisotropic, layered halfspaces. Journal of Engineering Mechanics, ASCE 115, 509–524.

Yan, B., Liu, Z., Zhang, X., 1999. Finite element analysis of wave propagation in fluid-saturated porous media. Applied Mathematics and Mechanics 20, 1331–1341.

Zeng, X., Rajapakse, R., 1999. Vertical vibrations of a rigid disk embedded in a poroelastic medium. Journal for Numerical and Analytical Methods in Geomechanics 23, 2075–2095.